NANO LETTERS

Letter

pubs.acs.org/NanoLett

Edge-Modified Phosphorene Nanoflake Heterojunctions as Highly Efficient Solar Cells

Wei Hu,[*,†] Lin Lin,[*,‡,†] Chao Yang,[*,†] Jun Dai,[§] and Jinlong Yang[*,∥]

[†]Computational Research Division, Lawrence Berkeley National Laboratory, 1 Cyclotron Road, Berkeley, California 94720, United States

[‡]Department of Mathematics, University of California, 1083 Evans Hall, Berkeley, California 94720, United States

[§]Department of Chemistry and Department of Mechanical and Materials Engineering, University of Nebraska-Lincoln, 536 Hamilton Hall, Lincoln, Nebraska 68588, United States

[∥]Hefei National Laboratory for Physical Sciences at Microscale, Department of Chemical Physics, and Synergetic Innovation Center of Quantum Information and Quantum Physics, University of Science and Technology of China, 96 JinZhai Road, Hefei, Anhui 230026, China

Supporting Information

ABSTRACT: We propose to use edge-modified phosphorene nanoflakes (PNFs) as donor and acceptor materials for heterojunction solar cells. By using density functional theory based calculations, we show that heterojunctions consisting of hydrogen- and fluorine-passivated PNFs have a number of desired optoelectronic properties that are suitable for use in a solar cell. We explain why these properties hold for these types of heterojunctions. Our calculations also predict that the maximum energy conversion efficiency of these type of heterojunctions, which can be easily fabricated, can be as high as 20%, making them extremely competitive with other types of two-dimensional heterojunctions.

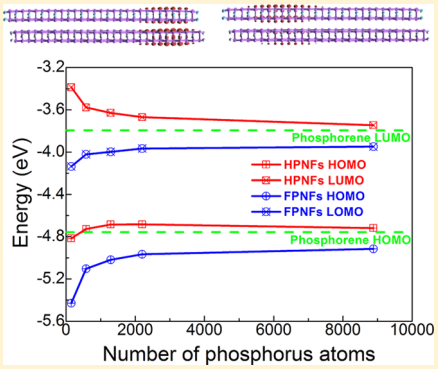

KEYWORDS: *Phosphorene nanoflakes, edge-modified, heterojunction solar cells, density functional theory*

Heterojunctions consisting of two types of donor and acceptor materials have been suggested as a promising mechanism for designing photovoltaics.[1−3] Choosing two different types of materials for donor and acceptor makes it possible to effectively separate charge carriers at the heterojunction interface. However, to be considered for use in a solar cell,the heterojunction must possess a number of other properties such as a small direct bandgap of roughly 1.2−1.6 eV[1] and a high electron mobility to facilitate efficient electron transport. The performance of such a heterojunction critically depends on the choice of donor and acceptor materials.[2]

In recent years, a number of two-dimensional (2D) materials[4−6] have been proposed as potential candidates to be used in heterojunctions.[7−11] Examples of heterojunction solar cells made from 2D materials include graphene/BN,[12] graphene/MoS_2,[13] MoS_2/$MoSe_2$,[14] MoS_2/g-C_3N_4,[15] and phosphorene/MoS_2.[16] One important and desirable feature of 2D materials is that they tend to have large photoreactive contact area for optical absorption. It is relatively easy to stack 2D materials up into multilayer systems with van der Waals interaction in between to further enhance sunlight capture.[17] The strong covalent bonds provide in-plane stability of each 2D monolayer, whereas the relatively weak van der Waals forces are sufficient to keep the stack together with their intrinsic optoelectronic properties preserved. Another reason why 2D materials have drawn a significant level of interest[4−6] is that they have been shown to exhibit tunable optoelectronic properties and high carrier mobility. In many ways, they are superior to conventional bulk solar-cell materials.[18] For example, graphene,[19] which is a 2D sp^2-hybridized carbon monolayer, has a high carrier mobility of up to 10^6 $cm^2/V/s$. MoS_2,[20] which is a representative 2D transition metal dichalcogenides (TMDCs), has a direct bandgap of 1.9 eV and a relatively high on−off current ratio of up to 10^8. However, some of these materials do not possess all desirable properties required in a solar cell. For example, graphene is metallic and does not have a bandgap, and the carrier mobility of MoS_2 is only 10^2 $cm^2/V/s$, which is much lower than that what is desired.

Phosphorene is an interesting and promising 2D elemental material[21−25] that has been isolated experimentally through mechanical exfoliation from bulk black phosphorus. Phosphorene exhibits some remarkable optoelectronic properties that are

Received: November 10, 2015
Revised: January 14, 2016
Published: February 5, 2016

DOI: 10.1021/acs.nanolett.5b04593
Nano Lett. 2016, 16, 1675−1682

superior to graphene and MoS_2. For example, phosphorene is a direct semiconductor with a high hole mobility[21] of 10^5 $cm^2/V/s$. When placed in nanoelectronics,[22,23] it exhibits drain current modulation of up to 10^5. It is the building block for black phosphorus quantum dots[24] that have been used to fabricate a flexible memory device with a high on−off current ratio of 6×10^4 and good stability. Furthermore, phosphorene possesses a thickness-dependent direct bandgap[21] in a wide range of 0.3 eV (bulk) to 1.5 eV (monolayer), which bridges the gap between graphene (0−0.2 eV) and MoS_2 (1.0−1.9 eV) for new optoelectronic devices. The thickness dependency of the bandgap allows one to tune the bandgap of phosphorene-based materials and enhance light absorption by varying the number of layers. Like graphene[26] and MoS_2,[27] phosphorene also has remarkable optical properties.[28] Therefore, phosphorene is an ideal candidate 2D material for solar cells.

In this paper, we propose a new way to construct a heterojunction from a single type of material derived from phosphorene only. The heterogeneity of the junction, which is critical for achieving charge separation, is introduced by using different types atoms to passivate nanoflakes cut out from the phosphorene. We show by density functional theory (DFT) based theoretical calculations that the electronic structures of phosphorene nanoflakes (PNFs) depend on the type of edge passivation. By using two different types of atoms to passivate the edges of the PNFs, we obtain two types of edge-modified PNFs that can be used as donor and acceptor materials in a heterojunction. Our computational results show that our proposed edge-modified PNF-based heterojunction has a desirable highest-occupied molecular orbital−lowest unoccupied molecular orbital (HOMO−LUMO) gap and optical absorption properties. The estimated maximum power conversion efficiency of this type of heterojunction can be as high as 20%, which is competitive with the efficiency of existing heterojunctions. We explain why these properties hold by using a surface dipole model.

Theoretical Models. When phospherene is cut into nanoflakes, edge passivation is required to stabilize the nanoflakes.[29,30] Different types of atoms can be used to passivate the edges of a nanoflake. Here we focus on rectangular PNFs that are passivated by either hydrogen atoms (HPNFs) or fluorine atoms (FPNFs). Figure 1a shows the atomic configuration of a 2D phosphorene monolayer in a 5×7 supercell (P_{140}). Some edge-passivated PNF nanoflakes we have examined include $P_{150}H_{34}$, $P_{150}F_{34}$, $P_{580}H_{68}$, $P_{580}F_{68}$, $P_{1290}H_{102}$, $P_{1290}F_{102}$, $P_{2200}H_{134}$, $P_{2200}F_{134}$, $P_{8880}H_{270}$, and $P_{8880}F_{270}$.

Hydrogen and fluorine edge passivation introduces polar covalent bonds of the forms P^--H^+ and P^+-F^-, respectively around the edges of the PNFs. These covalent bonds create edge dipole layers that produce constant electric potential jumps $\phi(\vec{r})$ in the form of $p/2\sqrt{2}\pi\varepsilon|\vec{r}| < |\phi(\vec{r})| < p/2\pi\varepsilon|\vec{r}|$ inside PNFs as shown in Figure 1(b) and (c), where $\vec{r}$ is the distance close to the edges and p represents the electric dipole moment per unit area at armchair and zigzag edges of PNFs. Such a potential jump shifts all single particle energy levels, including the HOMO and LUMO energies. The direction of the shift is different for HPNFs than it is for FPNFs. To be specific, the HOMO and LUMO levels of HPNFs are shifted upward upon edge passivation, whereas those associated with FPNFs are shifted downward.

This strong edge decoration effect on the HOMO and LUMO energy levels of PNFs makes it possible to design

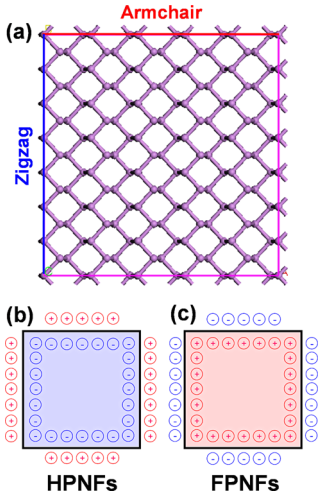

Figure 1. Geometric models for 2D phosphorene and PNFs. (a) Geometric structures of 2D phosphorene in a 5×7 supercell. The violet balls denote phosphorus atoms. Two types of edges, armchair and zigzag, are highlighted in the inset. Electric potential jumps produced by edge dipole layers of (b) HPNFs and (c) FPNFs, respectively. The red and blue regions indicate potential increase and decrease, respectively. Two circles represent electron and hole carriers at the electric dipole layer, respectively.

tunable and effective PNF based heterojunctions that are suitable for solar-cell devices. The opposite directions of the HOMO and LUMO energy shifts associated with HPNFs and FPNFs create a HOMO/LUMO offset when a monolayer of HPNF is placed adjacent to a monolayer of FPNF. Such an offset effectively reduces the HOMO/LUMO gap of the overall system through band alignment. It allows us to create a PNF heterobilayer that serves as a type-II donor−acceptor interface band heterojunction,[31] as illustrated in Figure 2. Furthermore,

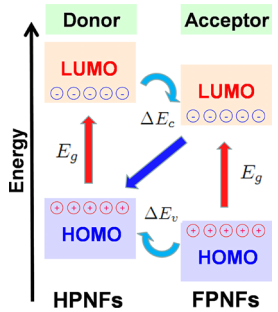

Figure 2. Schematic illustration of type-II donor−acceptor band alignments for the carrier transfer and separation in hybrid HPNF/FPNF heterobilayers. E_g is the band gap of PNFs. ΔE_c and ΔE_v represent the conduction and valence band offsets, respectively.

we predict that such type of heterojunction will promote electron and hole carrier transfer and separation at the HPNF/FPNF interface due to the built-in potential induced by the edge dipole layers inside monolayers. Such an induced potential is likely to localize HOMO and LUMO states within distinctive donor and acceptor regions. It is the localization of the HOMO and LUMO states that ultimately leads to enhanced charge separation and enables electron and hole carriers to be easily collected. These properties will lead to improved carrier lifetime when the heterojunction is used in solar cells.[32]

DOI: 10.1021/acs.nanolett.5b04593
Nano Lett. 2016, 16, 1675−1682

Results and Discussion. We now report computational results obtained from Kohn–Sham DFT based electronic structure analysis tools described in Computational Methods. We show how these results validate the theoretical model we established in Theoretical Models.

Electronic Structures of PNFs. The relevant electronic properties of to be examined for PNFs include the Kohn–Sham single particle energy levels, the local density of states (LDOS) near the HOMO and LUMO energy levels, and the projected density of state (PDOS) associated with phosphorus, hydrogen, or fluorine atoms.

To ascertain the effect of edge passivation on the electronic properties of PNFs, we first compute as a baseline for comparison the energy levels and the PDOS associated with a phosphorus atom for a 2D phosphorene placed in the 5 × 7 supercell (P_{140}) shown in Figure 3. We observe that

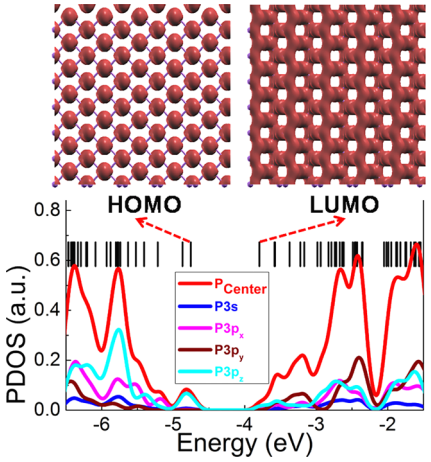

Figure 3. Energy levels of phosphorene and PDOS of equivalent phosphorus atom (denoted as P_{Center}) in the 5 × 7 supercell of phosphorene (P_{140}). Their LDOS of HOMO and LUMO are shown in the figure. The violet balls denote phosphorus atoms. All energy levels are referenced to the vacuum level, which is set to zero.

phosphorene is semiconducting with a direct band gap of 0.96 (GGA-PBE) or 1.52 (HSE06) eV.[29] The highest occupied molecular orbital (HOMO) and lowest unoccupied molecular orbital (LUMO) of P_{140} exhibit different electron distribution patterns. The HOMO states are found to consist of only $P3p_z$ orbitals associated with lone pairs of electrons, whereas the LUMO states are contributed by the sp^3 hybridized orbitals of P3s, $P3p_x$, $P3p_y$, and $P3p_z$. These particular features of the HOMO and LUMO orbitals suggest that the phosphorus atoms in phosphorene form three P–P σ-bonds and a nonbonding lone pair of electrons via asymmetric sp^3 hybridization of P3s, $P3p_x$, $P3p_y$, and $P3p_z$ atomic orbitals. When H or F atoms are used to passivate the edges of PNFs after they are cut out from phosphorene, P–H or P–F σ-bonds are expected to form around the edges. Figure 4, which illustrates how molecular orbital energies change through hybridization, shows that the molecular orbitals associated with these bonds, which characterizes the distribution of electrons around the edges of the PNFs and sometimes referred to as edge states, should be more stable than those that are composed of sp^3 hybridization orbitals of phosphorus atoms only. As a result, the corresponding molecular orbital energies are lower compared to those that characterize the sp^3 hybridization of the atomic orbitals associated with the P

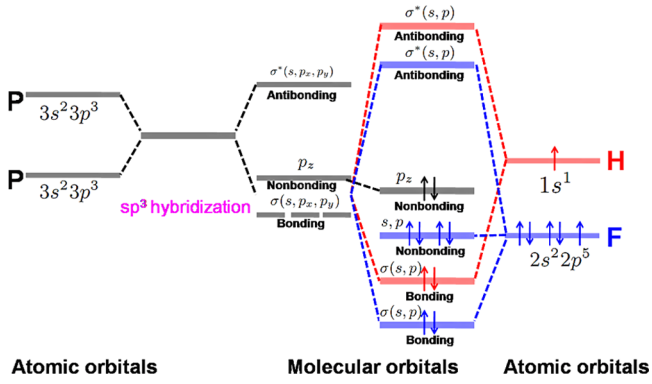

Figure 4. Schematic illustration of hybrid molecular orbital diagram for P–P, P–H, and P–F bonds in phosphorene and PNFs monolayers in different edge types. s, p_x, p_y, and p_z represent the atomic orbitals. σ and σ^* represent the bonding and antibonding molecular orbitals.

atoms in the interior of the PNFs. Therefore, they should not appear as HOMO or LUMO states of a PNF. In other words, the HOMO and LUMO states of a PNF should only be contributed by inner phosphorus atoms.

The predicted absence of edges states in the HOMO and LUMO range is verified by our computational results presented in Figure 5, which depict the energy levels and PDOS of PNFs monolayers of different sizes and with different types passivated edges. Their LDOS near the HOMO and LUMO are also shown. We can clearly see that the HOMO and LUMO states of both HPNFs and FPNFs share similar characteristics with those of a 2D phosphorene (P_{140}). In particular, unlike the widely studied GNFs,[33−36] none of the states around the HOMO and LUMO levels shows high density near the edges, that is, the HOMO and LUMO states do not contain any edge states. In fact, the densities of all HOMO and LUMO states appear to be contributed to only by inner phosphorus atoms. Therefore, for large-scale PNFs the difference in passivated edge types should have little effect on the HOMO/LUMO gaps of PNFs, which are close to that (0.96 eV) of a phosphorene.

Another indication that edge states do not contribute to the HOMO and LUMO of monolayer PNFs is that the change of the HOMO–LUMO energy gap with respect to the size of the PNF (L) becomes very small when L is beyond a certain size. This can be seen from Figure 6a in which the calculated HOMO–LUMO energy gaps E_g (eV) for PNFs of different sizes L (nm) are plotted. Our calculations show that the HOMO–LUMO gaps of HPNFs and FPNFs both increase linearly with respect to $1/L$. By using a linear least-squares fitting procedure, we obtain $E_g \approx 0.89 + 4.83/L$ for HPNFs and $E_g \approx 0.89 + 3.61/L$ for FPNFs, respectively. Therefore, when L is sufficiently large, the second term in these expressions becomes extremely small so that the HOMO/LUMO energy gap is mostly determined by the first constant, which is around 0.89 eV. Such a relationship between E_g and L is quite different from that associated with other low dimensional materials such as GNFs,[33−36] GNRs,[37−41] and boron nitride nanoribbons.[42−44] For these materials, the HOMO/LUMO states are dominated by edge states, and the HOMO/LUMO gap (E_g) can be smaller than that of bulk systems when L is sufficiently large. Unlike these materials, the small variation of the E_g associated with an edge passivated monolayer of PNF with respect to L for large L is mainly due to the well-known quantum confinement effect (QCE), which is present in most nanomaterials.

DOI: 10.1021/acs.nanolett.5b04593
Nano Lett. 2016, 16, 1675−1682

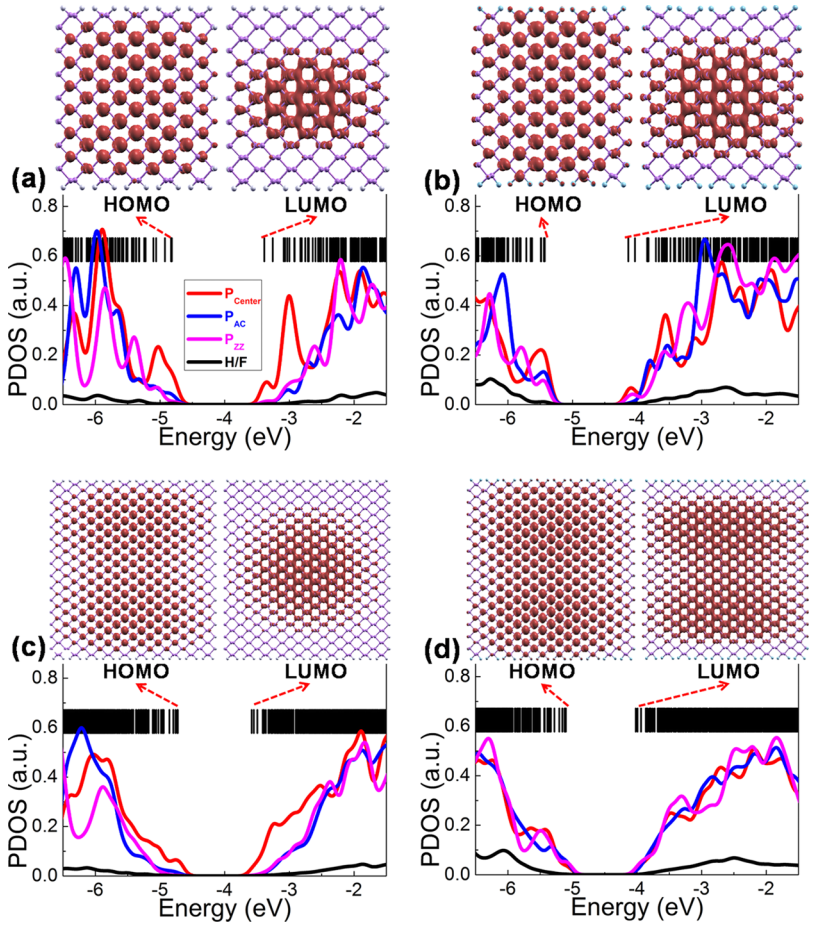

Figure 5. Energy levels and PDOS of PNF monolayers in different sizes and passivated edge types. (a) $P_{150}H_{34}$, (b) $P_{150}F_{34}$, (c) $P_{580}H_{68}$, and (d) $P_{580}F_{68}$, including the PDOS per atom of central phosphorus atom (P_{Center}), AC and ZZ edge phosphorus atoms (P_{AC} and P_{ZZ}), and hydrogen or fluorine atoms (H/F). Their LDOS of HOMO and LUMO are shown in the figure. All the energy levels are referenced to the vacuum level, which is set to zero. The violet, white, and blue balls denote phosphorus, hydrogen, and fluorine atoms, respectively.

Although the HOMO/LUMO bandgap of PNFs appears to be insensitive to the type of edge passivation, it is interesting to see from Figure 6b that the absolute HOMO and LUMO energy levels of a HPNF are different from those of a FPNF even when these PNFs contain nearly 10 000 atoms. Therefore, edge decoration appears to have a strong effect on the absolute HOMO and LUMO energies of PNFs. This observation is consistent with the prediction we made in Theoretical Models, which is based on the edge dipole layer model. Different types of passivated edges in PNFs can shift the orbital energy in different ways. Figure 6b shows that hydrogen edge passivation shifts the HOMO and LUMO energies up respectively by 0.04 and 0.05 eV from those of a phosphorene, whereas fluorine edge passivation shifts the HOMO and LUMO energies down respectively by 0.08 and 0.16 eV from those of a phosphorene. The difference in the amount of energy shift is Because polar covalent bond P^+-F^- in FPNFs has a stronger dipole moment than that of P^--H^+ in HPNFs. Hence, the HOMO and LUMO energy shifts (−0.08/−0.10 eV) of FPNFs are larger than those (0.04/0.05 eV) of HPNFs, respectively.

Heterobilayers of PNFs. As we indicated in Theoretical Models, by placing a monolayer of HPNF next to a monolayer of FPNF, we may obtain a heterobilayer with a reduced HOMO/LUMO bandgap compared to that of a PNF monolayer. The reduced bandgap results from a band alignment process[31] induced by the opposite directions of HOMO/LUMO energy shifts associated with hydrogenand fluorine edge passivation. It is consistent with the theory established for interlayer interactions.[16]

Such bandgap reduction is confirmed by our computation in which electronic properties two PNF heterobilayers ($P_{150}H_{34}$/$P_{150}F_{34}$ and $P_{580}H_{68}$/$P_{580}F_{68}$) are examined. These heterobilayers are generated by AB-stacking hydrogen and fluorine edge-passivated PNFs monolayers as shown in Figure 7. We used SIESTA-PEXSI to optimize the atomic positions of these heterobilayers. We observe that the bandgap of $P_{150}H_{34}$/$P_{150}F_{34}$ and $P_{580}H_{68}$/$P_{580}F_{68}$ is 0.93 and 0.70 eV, respectively. They are much smaller than the bandgap values associated with each constituent PNF monolayers (1.43, 1.29, 1.15, and 1.08 eV respectively for $P_{150}H_{34}$, $P_{150}F_{34}$, $P_{580}H_{68}$, and $P_{580}F_{68}$), as we predicted in Theoretical Models. The distribution of the single-particle energy levels associated with these two model heterobilayers, as well as their TDOS of PNF monolayers and heterobilayers are also shown in Figure 7.

The reduced bandgap in a heterobilayer of edge-modified PNFs increases the its absorption energy range and makes it easier for it to absorb visible light. Furthermore, interlayer interactions[45] and charge transfer[46] in such heterostructures can induce new optical transitions that result from the overlap of electronic states and enhance the absorption efficiency for hybrid HPNF and FPNF heterobilayers. These enhancements can be measured by examining the optical absorption

DOI: 10.1021/acs.nanolett.5b04593
Nano Lett. 2016, 16, 1675−1682

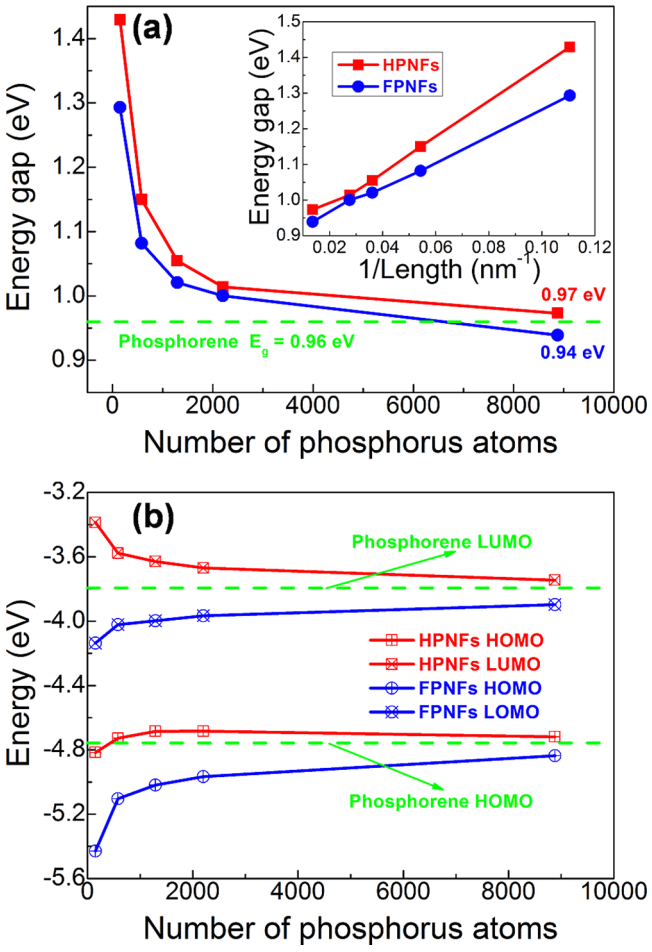

Figure 6. Energy gaps and HOMO and LUMO energies of large PNF monolayers in different system sizes and edge types. The energy gap and HOMO and LUMO energies of 2D phosphorene are marked by green dotted lines.

coefficients of PNF heterobilayers. Figure 8 shows that PNF heterobilayers exhibit a wider absorption range and stronger optical absorption compared to FPNF and HPNF monolayers. Furthermore, two monolayers in the same size show similar absorption spectrum due to the absence of edge states in FPNF and HPNF monolayers.

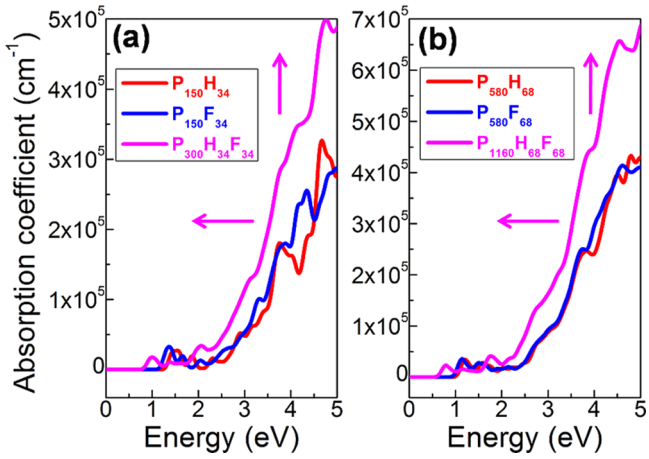

Figure 8. Absorption coefficients of PNFs monolayers and heterobilayers in different system sizes and edge types. (a) $P_{150}H_{34}$, $P_{150}F_{34}$ and $P_{300}H_{34}F_{34}$ ($P_{150}H_{34}/P_{150}F_{34}$). (b) $P_{580}H_{68}$, $P_{580}F_{68}$ and $P_{1160}H_{68}F_{68}$ ($P_{580}H_{68}/P_{580}F_{68}$). The wider absorption range and stronger optical absorption of PNF heterobilayers are marked by pink arrows.

Upon light absorption, electron and hole pairs are created at the interface between HPNF and FPNF. It follows from the type-II heterojunction alignment model[31] that the excited electrons tend to migrate from the HPNF layer to the FPNF layer due to the elevated electrostatic potential in the HPNF layer. For the same reason, holes tend to migrate from the FPNF layer to the FPNF layer due to the reduced the electrostatic potential on the FPNF side. As we indicated in

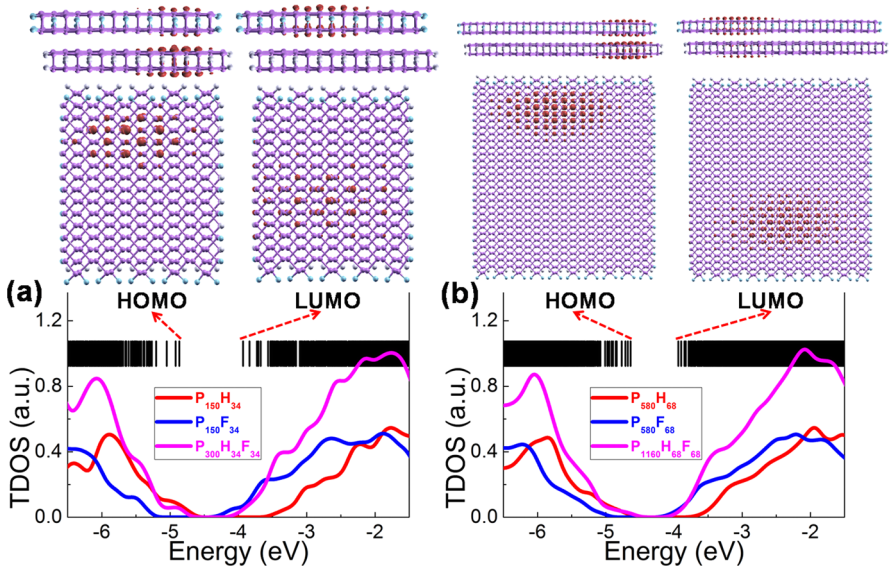

Figure 7. Energy levels and TDOS per atom of PNF heterobilayers in different system sizes and edge types. (a) $P_{300}H_{34}F_{34}$ and (b) $P_{1160}H_{68}F_{68}$. Corresponding PNF monolayers' TDOS also are shown in the figures, including $P_{150}H_{34}$, $P_{150}F_{34}$, $P_{580}H_{68}$, and $P_{580}F_{68}$. The LDOS of HOMO and LUMO of PNF heterobilayers are shown in the figure. All the energy levels are referenced to the vacuum level, which is set to zero. The violet, white, and blue balls denote phosphorus, hydrogen, and fluorine atoms, respectively.

DOI: 10.1021/acs.nanolett.5b04593
Nano Lett. 2016, 16, 1675−1682

Theoretical Models, these electron and hole migrations are likely to result in well-localized HOMO and LUMO states in a PNF heterobilayer. In particular, the HOMO states should be localized closer to the hydrogen passivated armchair edges in in-plane HPNF layers whereas the LUMO states should be localized closer to fluorine passivated armchair edges in in-plane FPNF layers. This type of localization can be easily observed in Figure 7 where the LDOS of the states near the HOMO and LUMO levels of both $P_{300}H_{34}F_{34}$ and $P_{1160}H_{68}F_{68}$ are shown.

The separation of the electron (LUMO) and hole (HOMO) states can also be revealed by examining the differential charge density ($\Delta\rho = \rho(\text{HPNFs/FPNFs}) - \rho(\text{HPNFs}) - \rho(\text{FPNFs})$) between the HPNF and FPNF layers. Figure 9 shows that

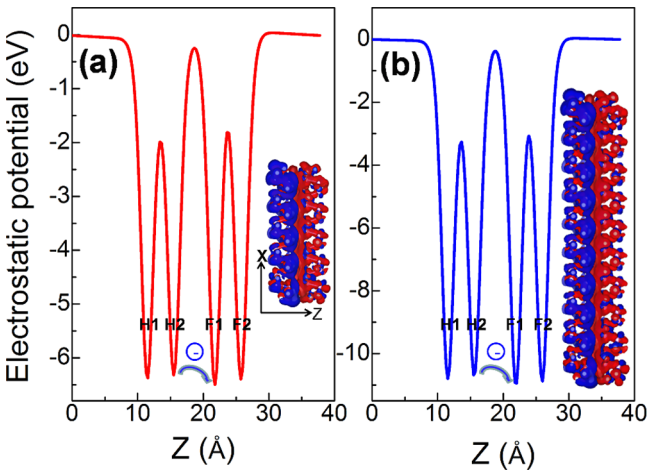

Figure 9. *XY*-averaged electrostatic potentials of heterobilayers of PNFs in different system sizes and edge types. (a) $P_{300}H_{34}F_{34}$ ($P_{150}H_{34}/P_{150}F_{34}$) and (b) $P_{1160}H_{68}F_{68}$ ($P_{580}H_{68}/P_{580}F_{68}$). Different hydrogen and fluorine edge-passivated layers in heterojunctions are marked by H1, H2, F1, and F2, respectively. Electrons transfer from the HPNFs H2 layer to the FPNFs F1 layer is marked in the figure. The differential charge density is shown in the figure. The red and blue regions indicate electron decrease and increase, respectively.

electron transfer from the HPNF layers to the FPNF layers with holes left on the HPNF layers, resulting in well-separated electron–hole pairs at the HPNF/FPNF interfaces.

From a practical perspective, the quality of heterojunction solar cells depends on its power conversion efficiency (PCE) defined as[12]

$$\eta = \frac{0.65(E_g - \Delta E_c - 0.3)\int_{E_g}^{\infty} \frac{P(\hbar\varpi)}{\hbar\varpi} d(\hbar\varpi)}{\int_0^{\infty} P(\hbar\varpi) d(\hbar\varpi)}$$

where 0.65 is the band-fill factor, $P(\hbar\varpi)$ is the AM1.5 solar energy flux at the photon energy $\hbar\varpi$, E_g is the bandgap of the donor, ΔE_c is the conduction band offsets, and the $(E_g - \Delta E_c - 0.3)$ term is an estimation of the maximum open circuit voltage.

The maximum PCE depends critically on the interface band alignment between donor and acceptor materials.[12] For large-scale hybrid HPNF/FPNF heterobilayers, the bandgap values E_g of donor and acceptor monolayers are the same, and they are equal to that (E_g = 1.52 eV (HSE06)[29]) of 2D phosphorene. This gap value is very suitable for the absorption of the solar spectrum[12] and can be tuned by changing the number of layers in multilayer phosphorene.[21] The conduction band offset ΔE_c between large-scale HPNFs and FPNFs up to 9150 atoms is ΔE_c = 0.15 eV, which are close to optimal values of conduction band offset to archive the high PCE in heterojunction solar cells.[16] Therefore, large-scale HPNF/FPNF heterobilayers can achieve PCE as high as 20%. These values are comparable to that of recently proposed bilayer phosphorene/MoS_2 heterojunctions (16–18%),[16] hybrid PCBM/CBN heterojunctions (10–20%)[12] and g-SiC_2 based systems (12–20%)[47] for highly efficient solar cells.

It is important to recognize that larger-scale PNF heterobilayers' conduction band offsets can be effectively and precisely engineered by edge passivation. What is unique for PNFs is that edge modification does not alter certain electronic properties such as band gap and carrier mobility. These electronic properties also do not depend sensitively on the system size. Furthermore, we expect that large-scale HPNF/FPNF heterobilayers can be easily fabricated because two PNF monolayers can be stacked or combined with weak van der Waals interaction. Since the donor and acceptor are both derived from phosphorene with different types edge passivation, we do not need to be concerned with lattice mismatch and Moiré effect[48] between HPNF and FPNF monolayers. Although we considered thin bilayer PNFs with potential application in solar-cell devices, it is also possible to devise thicker multilayer PNF heterojunctions that can be further optimized to increase the photoreactive contact interface area and to enhance the range of light absorption. These improvement can lead to higher PCEs in practical applications. On the other hand, our proposed edge-modifiled PNF heterojunction model can be universally extended and applied to a variety of 1D and 2D systems, such as GNFs,[33−36] GNRs,[37−41] and PNRs.[49−51] Therefore, this edge-modified 2D heterojunction model may lead to new semiconductor optoelectronic devices in the future experiments, especially for ultrathin solar cells.[12,16,47]

Conclusion. We propose to use edge-modified phospherene nanoflakes to create donor and acceptor materials that can be used in a heterojunction solar cell. Our DFT-based theoretical calculations indicate that the HOMO and LUMO energy levels of PNFs shift away from those of bulk phosphorene in different directions when they are passivated with H atoms and F atoms, respectively. When a HPNF monolayer is placed next to a FPNF layer to form a heterobilayer, the opposite shifts of the HOMO and LUMO energy levels associated with the HPNF and FPNF monolayers result in an overall reduced HOMO/LUMO energy gap for the heterobilayer through a band alignment process. We examined the HOMO/LUMO states of the heterobilayer and showed that they are localized in the donor and acceptor region, respectively. The localized HOMO and LUMO states indicate that charge separation can be effective achieve at the heterojunction interface. We explained why these electronic properties hold by using a surface dipole model to elucidate the electronic structure of PNFs. In particular, we explain the absence of edge states near the HOMO/LUMO region of edge modified PNFs. Our calculations also predict that a heterojunction consisting of HPNF and FPNF can achieve a maximum power conversion efficiency of up to 20%, which is competitive with other types of 2D heterojunctions. Because edge-modified PNF heterojunctions can be easily fabricated without no lattice mismatch and Moiré effect, we believe they are extremely suitable for building high efficiency and low cost solar cells.

DOI: 10.1021/acs.nanolett.5b04593
Nano Lett. 2016, 16, 1675−1682

Computational Methods. We use the Kohn−Sham DFT-based electronic structure analysis tools implemented in the Spanish Initiative for Electronic Simulations with Thousands of Atoms (SIESTA)[52] software package to study the optoelectronic properties of PNFs and verify our prediction discussed above. We choose the generalized gradient approximation of Perdew, Burke, and Ernzerhof (GGA-PBE)[53] exchange correlation functional, which generally gives a good description of electronic structures of phosphorene,[21] graphene nanoflakes (GNFs),[54] graphene nanoribbons (GNRs),[55] and phosphorene nanoribbons (PNRs).[29] We adopt the van der Waals correction proposed by Grimme (DFT-D2)[56] to optimize the layered atomic structures of PNF heterojunctions. We use the double-ζ plus polarization orbital basis set (DZP) to describe the valence electrons within the framework of a linear combination of numerical atomic orbitals (LCAO).[57] All atomic coordinates are fully relaxed using the conjugate gradient (CG) algorithm until the energy and force convergence criteria of 10^{-4} eV and 0.04 eV/Å, respectively, are reached. Our results for the atomic structures and electronic properties of 2D phosphorene (P_{140}) in the 5 × 7 supercell and PNFs ($P_{150}H_{34}$ and $P_{150}F_{34}$) are crosschecked with Vienna Ab initio Simulation Package (VASP)[58] calculations. Because the GGA-PBE exchange correlation functional tends to underestimate the bandgap of semiconductors, the screened hybrid HSE06 functional[59] implemented in VASP is also used to check the electronic band structure of phosphorene.

Because of the large number of atoms contained in the PNFs under study, the standard diagonalization (DIAGON) method in SIESTA, which is based on the ScaLAPACK[60] software package, becomes prohibitively expensive. Therefore, we use the recently developed Pole EXpansion and Selected Inversion (PEXSI) technique[61−64] to reduce the computational time without sacrificing accuracy even for metallic systems. The PEXSI technique allows the evaluation of physical quantities such as electron density, total energy, and atomic forces to be performed without calculating any eigenvalue or eigenfunction. Furthermore, the SIESTA-PEXSI method can scale to more than 10 000 processors on high-performance computing machines.

We use the first-order time-dependent perturbation theory implemented in SIESTA[52] to study the optical properties of large-scales PNF monolayers and heterobilayers. We crosscheck the optical properties of phosphorene against previous theoretical calculations.[28]

■ ASSOCIATED CONTENT

Supporting Information

The Supporting Information is available free of charge on the ACS Publications website at DOI: 10.1021/acs.nanolett.5b04593.

Table of SIESTA-PEXSI calculated equilibrium interfacial distance and binding energy per atom Eb for different bilayers of PNFs, figure of energy gaps of bilayer phosphorene and HPNF/FPNF heterobilayer $P_{300}H_{34}F_{34}$ as a function of interlayer distance, and figure of electronic properties of HPNF/FPNF heterobilayer $P_{300}H_{34}F_{34}$ in different stacking configurations. (PDF)

■ AUTHOR INFORMATION

Corresponding Authors

*(W.H.): Phone: +1-5105416034. E-mail: whu@lbl.gov.

*(L.L.): Phone: +1-5106647189. E-mail: linlin@math.berkeley.edu.

*(C.Y.): Phone: +1-5104866424. E-mail: cyang@lbl.gov.

*(J.Y.): Phone: +86-55163606408. E-mail: jlyang@ustc.edu.cn.

Notes

The authors declare no competing financial interest.

■ ACKNOWLEDGMENTS

This work is partially supported by the Scientific Discovery through Advanced Computing (SciDAC) Program funded by U.S. Department of Energy, Office of Science, Advanced Scientific Computing Research and Basic Energy Sciences (W.H., L.L. and C.Y.) and by the Center for Applied Mathematics for Energy Research Applications (CAMERA), which is a partnership between Basic Energy Sciences and Advanced Scientific Computing Research at the U.S Department of Energy (L.L. and C.Y.). We thank the National Energy Research Scientific Computing (NERSC) center for the computational resources. This work is also partially supported by the National Key Basic Research Program (2011CB921404), by NSFC (21421063, 91021004, 21233007), by Chinese Academy of Sciences (CAS) (XDB01020300), and by USTCSCC, SCCAS, Tianjin, and Shanghai Supercomputer Centers.

■ REFERENCES

(1) Shockley, W.; Queisser, H. J. *J. Appl. Phys.* **1961**, *32*, 510.
(2) Scharber, M. C.; Mühlbacher, D.; Koppe, M.; Denk, P.; Waldauf, C.; Heeger, A. J.; Brabec, C. J. *Adv. Mater.* **2006**, *18*, 789−794.
(3) Graetzel, M.; Janssen, R. A. J.; Mitzi, D. B.; Sargent, E. H. *Nature* **2012**, *488*, 304−312.
(4) Novoselov, K. S.; Jiang, D.; Schedin, F.; Booth, T. J.; Khotkevich, V. V.; Morozov, S. V.; Geim, A. K. *Proc. Natl. Acad. Sci. U. S. A.* **2005**, *102*, 10451.
(5) Osada, M.; Sasaki, T. *Adv. Mater.* **2012**, *24*, 210.
(6) Xu, M.; Liang, T.; Shi, M.; Chen, H. *Chem. Rev.* **2013**, *113*, 3766.
(7) Dean, C.; Young, A. F.; Wang, L.; Meric, I.; Lee, G.-H.; Watanabe, K.; Taniguchi, T.; Shepard, K.; Kim, P.; Hone, J. *Solid State Commun.* **2012**, *152*, 1275−1282.
(8) Geim, A. K.; Grigorieva, I. V. *Nature* **2013**, *499*, 419−425.
(9) Wang, H.; Liu, F.; Fu, W.; Fang, Z.; Zhou, W.; Liu, Z. *Nanoscale* **2014**, *6*, 12250−12272.
(10) Niu, T.; Li, A. *Prog. Surf. Sci.* **2015**, *90*, 21−45.
(11) Hu, W.; Yang, J. *Comput. Mater. Sci.* **2015**, *102*, 208.
(12) Bernardi, M.; Palummo, M.; Grossman, J. C. *ACS Nano* **2012**, *6*, 10082−10089.
(13) Bernardi, M.; Palummo, M.; Grossman, J. C. *Nano Lett.* **2013**, *13*, 3664−3670.
(14) Ceballos, F.; Bellus, M. Z.; Chiu, H.-Y.; Zhao, H. *ACS Nano* **2014**, *8*, 12717−12724.
(15) Wang, J.; Guan, Z.; Huang, J.; Li, Q.; Yang, J. *J. Mater. Chem. A* **2014**, *2*, 7960−7966.
(16) Dai, J.; Zeng, X. C. *J. Phys. Chem. Lett.* **2014**, *5*, 1289−1293.
(17) Li, X.; Zhu, H.; Wang, K.; Cao, A.; Wei, J.; Li, C.; Jia, Y.; Li, Z.; Li, X.; Wu, D. *Adv. Mater.* **2010**, *22*, 2743−2748.
(18) Green, M. A.; Emery, K.; Hishikawa, Y.; Warta, W.; Dunlop, E. D. *Prog. Photovoltaics* **2015**, *23*, 1−9.
(19) Geim, A. K.; Novoselov, K. S. *Nat. Mater.* **2007**, *6*, 183−191.
(20) Radisavljevic, B.; Radenovic, A.; Brivio, J.; Giacometti, V.; Kis, A. *Nat. Nanotechnol.* **2011**, *6*, 147−150.
(21) Liu, H.; Neal, A. T.; Zhu, Z.; Luo, Z.; Xu, X.; Tománek, D.; Ye, P. D. *ACS Nano* **2014**, *8*, 4033−4041.
(22) Li, L.; Yu, Y.; Ye, G.; Ge, Q.; Ou, X.; Wu, H.; Feng, D.; Chen, X.; Zhang, Y. *Nat. Nanotechnol.* **2014**, *9*, 372−377.
(23) Das, S.; Zhang, W.; Demarteau, M.; Hoffmann, A.; Dubey, M.; Roelofs, A. *Nano Lett.* **2014**, *14*, 5733−5739.

DOI: 10.1021/acs.nanolett.5b04593
Nano Lett. 2016, 16, 1675−1682

(24) Zhang, X.; Xie, H.; Liu, Z.; Tan, C.; Luo, Z.; Li, H.; Lin, J.; Sun, L.; Chen, W.; Xu, Z.; Xie, L.; Huang, W.; Zhang, H. *Angew. Chem., Int. Ed.* **2015**, *54*, 3653−3657.
(25) Hu, W.; Wang, T.; Yang, J. *J. Mater. Chem. C* **2015**, *3*, 4756−4761.
(26) Bonaccorso, F.; Sun, Z.; Hasan, T.; Ferrari, A. C. *Nat. Photonics* **2010**, *4*, 611−622.
(27) Splendiani, A.; Sun, L.; Zhang, Y.; Li, T.; Kim, J.; Chim, C.-Y.; Galli, G.; Wang, F. *Nano Lett.* **2010**, *10*, 1271−1275.
(28) Qiao, J.; Kong, X.; Hu, Z.-X.; Yang, F.; Ji, W. *Nat. Commun.* **2014**, *5*, 4475.
(29) Guo, H.; Lu, N.; Dai, J.; Wu, X.; Zeng, X. C. *J. Phys. Chem. C* **2014**, *118*, 14051−14059.
(30) Hu, W.; Lin, L.; Yang, C. *Phys. Chem. Chem. Phys.* **2015**, *17*, 31397.
(31) Zhang, J.; Zhang, M.; Sun, R.-Q.; Wang, X. *Angew. Chem., Int. Ed.* **2012**, *51*, 10145−10149.
(32) Ma, J.; Wang, L.-W. *Nano Lett.* **2015**, *15*, 248−253.
(33) Zhou, Y.; Wang, Z.; Yang, P.; Sun, X.; Zu, X.; Gao, F. *J. Phys. Chem. C* **2012**, *116*, 5531−5537.
(34) Kim, S.; et al. *ACS Nano* **2012**, *6*, 8203−8208.
(35) Jin, S. H.; Kim, D. H.; Jun, G. H.; Hong, S. H.; Jeon, S. *ACS Nano* **2013**, *7*, 1239−1245.
(36) Hu, W.; Lin, L.; Yang, C.; Yang, J. *J. Chem. Phys.* **2014**, *141*, 214704.
(37) Barone, V.; Hod, O.; Scuseria, G. E. *Nano Lett.* **2006**, *6*, 2748−2754.
(38) Son, Y.-W.; Cohen, M. L.; Louie, S. G. *Phys. Rev. Lett.* **2006**, *97*, 216803.
(39) Kan, E.; Li, Z.; Yang, J.; Hou, J. G. *J. Am. Chem. Soc.* **2008**, *130*, 4224−4225.
(40) Li, X.; Wang, X.; Zhang, L.; Lee, S.; Dai, H. *Science* **2008**, *319*, 1229−1232.
(41) Jia, X.; Hofmann, M.; Meunier, V.; Sumpter, B. G.; Campos-Delgado, J.; Romo-Herrera, J. M.; Son, H.; Hsieh, Y.-P.; Reina, A.; Kong, J.; Terrones, M.; Dresselhaus, M. S. *Science* **2009**, *323*, 1701−1705.
(42) Park, C.-H.; Louie, S. G. *Nano Lett.* **2008**, *8*, 2200−2203.
(43) Topsakal, M.; Aktrk, E.; Ciraci, S. *Phys. Rev. B: Condens. Matter Mater. Phys.* **2009**, *79*, 115442.
(44) Mukherjee, R.; Bhowmick, S. *J. Chem. Theory Comput.* **2011**, *7*, 720−724.
(45) Wu, F.; Liu, Y.; Yu, G.; Shen, D.; Wang, Y.; Kan, E. *J. Phys. Chem. Lett.* **2012**, *3*, 3330−3334.
(46) Du, A.; Sanvito, S.; Li, Z.; Wang, D.; Jiao, Y.; Liao, T.; Sun, A.; Ng, Y. H.; Zhu, Z.; Amal, R.; Smith, S. C. *J. Am. Chem. Soc.* **2012**, *134*, 4393−4397.
(47) Zhou, L.-J.; Zhang, Y.-F.; Wu, L.-M. *Nano Lett.* **2013**, *13*, 5431−5436.
(48) Kang, J.; Li, J.; Li, S.-S.; Xia, J.-B.; Wang, L.-W. *Nano Lett.* **2013**, *13*, 5485−5490.
(49) Han, X.; Stewart, H. M.; Shevlin, S. A.; Catlow, C. R. A.; Guo, Z. X. *Nano Lett.* **2014**, *14*, 4607−4614.
(50) Kou, L.; Frauenheim, T.; Chen, C. *J. Phys. Chem. Lett.* **2014**, *5*, 2675−2681.
(51) Ramasubramaniam, A.; Muniz, A. R. *Phys. Rev. B: Condens. Matter Mater. Phys.* **2014**, *90*, 085424.
(52) Soler, J. M.; Artacho, E.; Gale, J. D.; García, A.; Junquera, J.; Ordejón, P.; Sánchez-Portal, D. *J. Phys.: Condens. Matter* **2002**, *14*, 2745.
(53) Perdew, J. P.; Burke, K.; Ernzerhof, M. *Phys. Rev. Lett.* **1996**, *77*, 3865.
(54) Kan, E.; Hu, W.; Xiao, C.; Lu, R.; Deng, K.; Yang, J.; Su, H. *J. Am. Chem. Soc.* **2012**, *134*, 5718−5721.
(55) Wassmann, T.; Seitsonen, A. P.; Saitta, A. M.; Lazzeri, M.; Mauri, F. *J. Am. Chem. Soc.* **2010**, *132*, 3440−3451.
(56) Grimme, S. *J. Comput. Chem.* **2006**, *27*, 1787−1799.
(57) Junquera, J.; Paz, O.; Sánchez-Portal, D.; Artacho, E. *Phys. Rev. B: Condens. Matter Mater. Phys.* **2001**, *64*, 235111.
(58) Kresse, G.; Hafner, J. *Phys. Rev. B: Condens. Matter Mater. Phys.* **1993**, *47*, 558.
(59) Heyd, J.; Scuseria, G. E.; Ernzerhof, M. *J. Chem. Phys.* **2006**, *124*, 219906.
(60) Auckenthaler, T.; Blum, V.; Bungartz, H. J.; Huckle, T.; Johanni, R.; Krämer, L.; Lang, B.; Lederer, H.; Willems, P. R. *Parallel Comput.* **2011**, *37*, 783−794.
(61) Lin, L.; Lu, J.; Ying, L.; Car, R.; Weinan, E. *Comm. Math. Sci.* **2009**, *7*, 755−777.
(62) Lin, L.; Chen, M.; Yang, C.; He, L. *J. Phys.: Condens. Matter* **2013**, *25*, 295501.
(63) Lin, L.; García, A.; Huhs, G.; Yang, C. *J. Phys.: Condens. Matter* **2014**, *26*, 305503.
(64) Hu, W.; Lin, L.; Yang, C. *J. Chem. Phys.* **2015**, *143*, 124110.

DOI: 10.1021/acs.nanolett.5b04593
Nano Lett. 2016, 16, 1675−1682